FULL PAPER

Tumor Microenvironment Activated Photothermal Strategy for Precisely Controlled Ablation of Solid Tumors upon NIR Irradiation

Enguo Ju, Kai Dong, Zhen Liu, Fang Pu, Jinsong Ren, and Xiaogang Qu**

Photothermal ablation has provided emerging and promising opportunities to further potentiate the efficacy of postoperative chemotherapy of tumor. However, it still cannot achieve a high level of selectivity because extraneous photodamage along the optical path to the tumor is unavoidable as the result of the uncontrollable distribution of the photothermal agents. In addition, it is technically difficult to keep photoirradiation localizing only on cancer cells. In this report, a new strategy is introduced for precisely controlled ablation of tumor through tumor microenvironment activated near-infrared (NIR) photothermal therapy. By taking advantage of the pH-dependent light-heat conversion property of Au@PANI nanoparticles, much higher photothermal effect at pH 6.5 than that at pH 7.4 is achieved. Therefore, in normal tissues and blood vessels, NIR irradiation cannot lead to a lethal temperature with little or no harm to normal cells. In contrast, in acidic tumor microenvironment, the photothermal effect is activated. Consequently, NIR irradiation can effectively kill cancer cells through local hyperthermia. Importantly, with the benefit of the internal and external control to switch on the photothermal ablation, the technical difficulty to precisely localize laser irradiation on tumor cells can be circumvented.

1. Introduction

Photothermal ablation with near-infrared (NIR) laser has provided emerging and promising opportunities to further potentiate the efficacy of postoperative chemotherapy of tumor.[1–3] As a minimally invasive therapy modalities, NIR possesses the advantages of transmitting through tissue with relatively little attenuation and favorable biosafety.[4–6] In addition, as an orthogonal external stimulus, NIR allows for spatial and temporal exposure in the tumor region to minimize the side effects. In the past decade, numerous smart nanostructures have been rational designed by integrating hyperthermia, chemotherapy, and imaging modalities into one for early cancer diagnosis and imaging-guided therapy.[7–15] Though great achievements have been made, it still cannot achieve a high level of selectivity because extraneous photo damage along the optical path to the tumor are unavoidable as the result of the uncontrollable distribution of the photothermal agents (especially in vascellum, liver, and spleen). In addition, it is technically difficult to keep photoirradiation localizing only on cancer cells.[16] Therefore, to minimize nonspecific thermal injury to normal tissues and to exert the maximum therapy effect in the region of tumor, a photothermal agent that has little phototoxicity in normal tissues while producing lethal effects over the target cancer cells is urgently required.

The recent advances in understanding the critical roles of the tumor microenvironment in tumor progression have resulted in emerging diagnostic and therapeutic agents designed and engineered specifically targeting the microenvironment components.[17–20] One well-known unique feather of most tumor physiology is acidosis. The extracellular pH of tumor is more acidic (pH 6.0–7.0) than that of extracellular fluid/blood in normal tissue (pH 7.2–7.4), which results from hypoxia, glycolysis, and ion channel disorder.[21–24] Herein, we introduce a new strategy for controlled precise ablation of tumor through activating NIR photothermal effect by the tumor acidic microenvironment (**Scheme 1**). The strategy employs the tumor microenvironment to activate the photothermal property of the agents and subsequently NIR laser irradiation can generate hyperthermia to ablate the tumor. During circulation in the blood or retention in normal tissues, the photothermal property of nanoparticles is not activated (photothermal effect "off"). Therefore, the blood vascellum or normal tissues can be protected even upon the irradiation of NIR laser. Once nanoparticles extravasated into tumor tissue, the photothermal effect is activated by the tumor microenvironment such as lower pH (photothermal effect "on"). As a result, the tumor cells can be effectively killed once irradiated with NIR laser. This strategy could provide highly discriminating photodamage to tumor cells, but not to normal tissues, thus circumventing the technical difficulty to precisely localize laser irradiation on tumor cells.

Previously, Haam's group reported convertible organic polyaniline (PANI) nanoparticles as a photothermal agent for

E. Ju, K. Dong, Z. Liu, F. Pu, Prof. J. Ren, Prof. X. Qu
Laboratory of Chemical Biology and State Key Laboratory of Rare Earth Resource Utilization
Changchun Institute of Applied Chemistry
Chinese Academy of Sciences
Changchun, Jilin 130022, P.R. China
E-mail: jren@ciac.ac.cn; xqu@ciac.ac.cn
E. Ju, K. Dong
University of Chinese Academy of Sciences
Beijing 100039, P.R. China

DOI: 10.1002/adfm.201403885

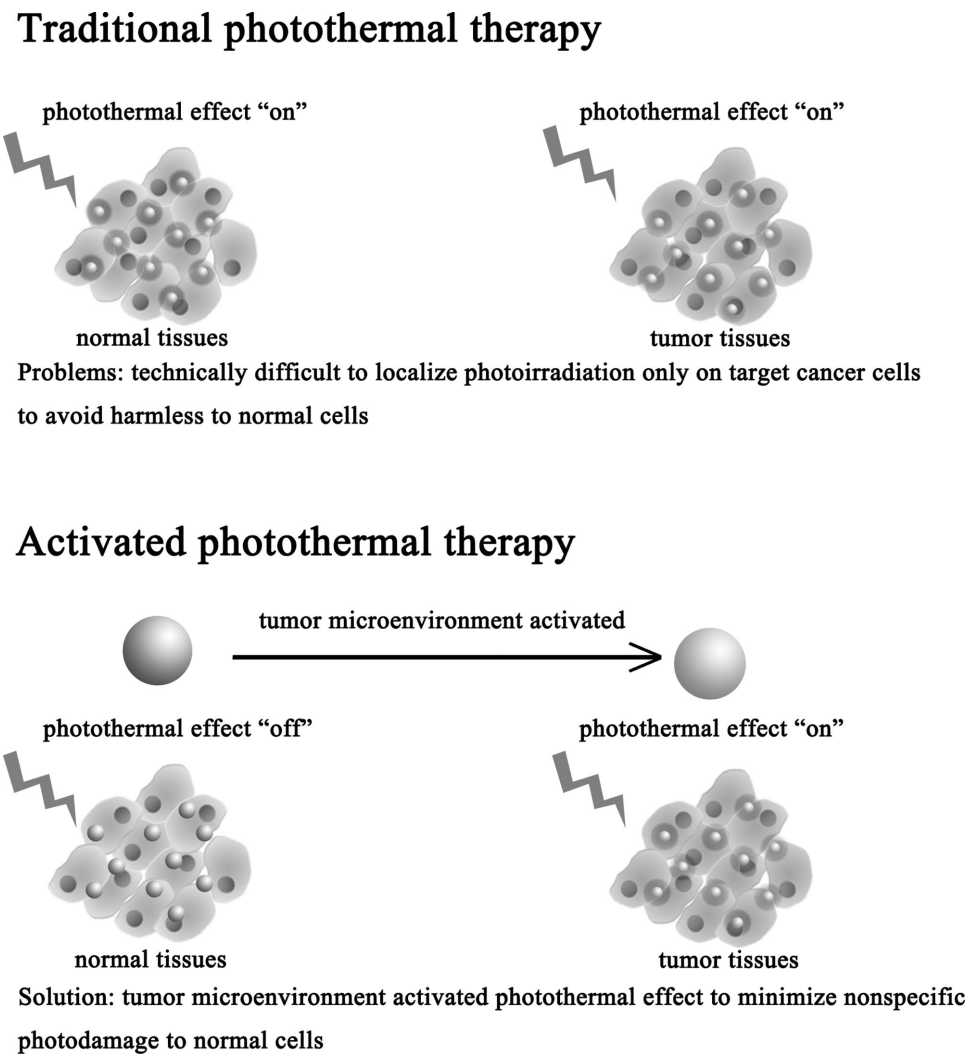

Scheme 1. Illustation of the traditional photothermal therapy and the activated photothermal therapy strategy.

photothermal ablation of epithelial cancer cells.[25,26] Interestingly, PANI in the form of emeraldine salt could raise the temperature to 60 °C upon NIR laser irradiation, while that in the form of emeraldine base at an equivalent concentration could only reach less than 40 °C with the same irradiation condition.[25] Unfortunately, the transition pH of emeraldine base to emeraldine salt was extremely low (pH < 3), which is difficult to be realized in tumor microenvironment. To shift the transition of PANI to a high pH environment, two principal strategies have been proposed up to date. One way is to introduce acidic groups into the PANI chains to hinder the deprotonation of its emeraldine salt form.[27–29] The other way is to incorporate conductive nanomaterials into PANI matrix to improve the charge transfer rate.[30–33] In this study, we reported the construction of PEGylationAu nanoparticle core/PANI shell nanostructures (Au@PANI) as tumor acidic microenvironment-activated photothermal agent for ablation of cancer cells. With the help of the charge transfer from AuNPs to PANI and doping process induced increased electron-delivery efficiency, Au@PANI showed much higher photothermal effect at pH 6.5 than that at pH 7.4. Therefore, in normal tissues and blood vessels, NIR irradiation could not lead to a lethal temperature with little or no harm to normal cells. In contrast, in acidic tumor microenvironment, the photothermal effect could be activated. Consequently, NIR irradiation could effectively kill cancer cells through local hyperthermia. Importantly, with the benefit of the internal and external control to switch on the photothermal ablation, the technical difficulty to precisely localize laser irradiation on tumor cells could be circumvented.

2. Results and Discussion

The encapsulation of AuNPs by PANI was achieved by mixing aqueous aniline, sodium dodecylsulfate (SDS), citrate-protected AuNPs, and acidic oxidant in sequence, followed by incubation for 12 h to complete polymerization (Figure S1, Supporting Information). In this process, the neutral aniline molecules with exocyclic amino group could strongly coordinate to AuNPs through ligand exchange with weakly bound negatively charged citrate ions.[34–36] SDS molecule was believed to embed its hydrophobic tail in the aniline layer, while the negative sulfate group

stabilized the NPs from aggregation. Upon the addition of oxidant, the polymerization occurred on the surface of the AuNPs to form PANI shell construction. Finally, PEGylation Au core/PANI shell nanoparticles (termed as Au@PANI) were obtained through the electrostatic interaction between negative charged nanoparticles and positive charged poly(ethylene glycol) bis(3-aminopropl) terminated. In our study, the AuNPs cores at three different sizes were also prepared. The obtained Au@PANI had a diameter of about 35, 45, and 65 nm with a shell thickness of around 11 nm and showed a good dispersity (**Figure 1**A–C and Figure S2, Supporting Information). The mass percents of Au in Au@PANI were increased as the size of Au core increased (Table S1, Supporting Information). To explore the sensitivity of Au@PANI to acidic environment, we next investigated their optical properties at different pH values. To ensure the final pH of the solution was the same as phosphate buffer (PB), 10 µL of the prepared Au@PANI was diluted by 4 mL PB buffer to minimize the influence of Au@PANI to the buffer pH. As shown in Figure 1D–F, the surface plasmon absorption shifted to above 540 nm from the original citrate protected AuNPs, indicating that the refractive index of the media surrounding the AuNPs surface changed. The absorbance in the NIR region resulted from the charge transfer between quinoid and benzenoid rings of PANI, where optical attenuation of tissue is relatively low and affords deep light penetration. With the decrease of the pH value, the absorptions in NIR region of three different sizes of Au@PANI were all increased, which was attributed to the doping process induced increased electron-delivery efficiency. Specially, Au@PANI with 16 nm core showed an absorbance peak at 800 nm at 6.5, while this peak disappeared at pH 7.4 and 8.0. Taking advantage of the peak position at 800 nm and the distinct absorbance between pH 7.4 and pH 6.5, we therefore took Au@PANI with 16 nm core as a representative to study the photothermal conversion in the following experiments. As shown in Figure 1G, Au@PANI in PB buffer with different pH were irradiated by 808 nm laser at a power density of 2 W cm^{-2} and the temperature were real-time recorded by temperature gauge or infrared camera. The optimum concentration was determined by the maximum temperature rise of Au@PANI at pH 7.4 to less than 40 °C. With the same concentration, we then replaced the buffer with the pH of 6.5 and observed that the temperature could rise to a value above 50 °C, which was beyond the temperature tolerance of cancer cells.[37–39] Considering the pH difference between normal tissues and tumor microenvironment, we hypothesized that Au@PANI under NIR laser irradiation showed stealth photothermal property in normal tissues while in tumor microenvironment the photothermal effect could be activated for hyperthermic killing of cancer cells.[40,41]

In order to clarify the mechanism of the pH-dependent photothermal effect, we next investigated the structure of

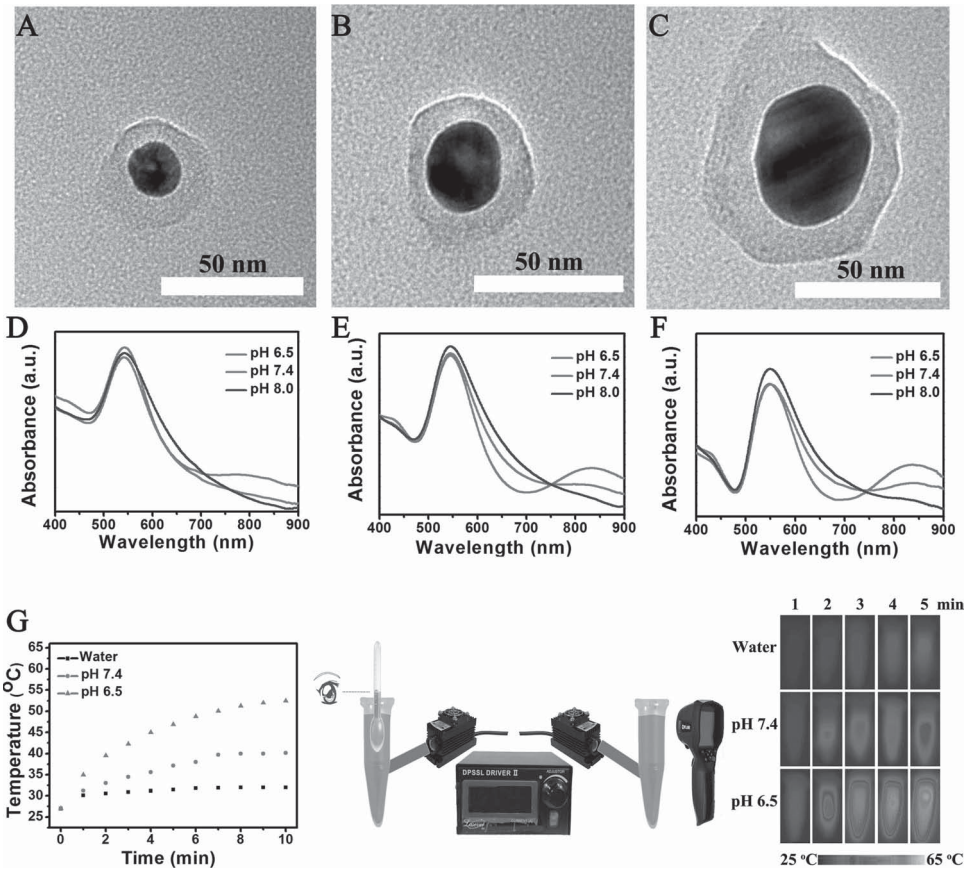

Figure 1. TEM images and the corresponding UV spectra in PB buffer with different pH of Au@PANI with the Au core of 16 nm (A,D); 24.5 nm (B,E); and 41 nm (C,F). G) Photothermal effect of Au@PANI (100 µg mL^{-1}) with 16 nm core in PB buffer with different pH under laser irradiation (808 nm, 2 W cm^{-2}) recorded by temperature gauge or infrared camera.

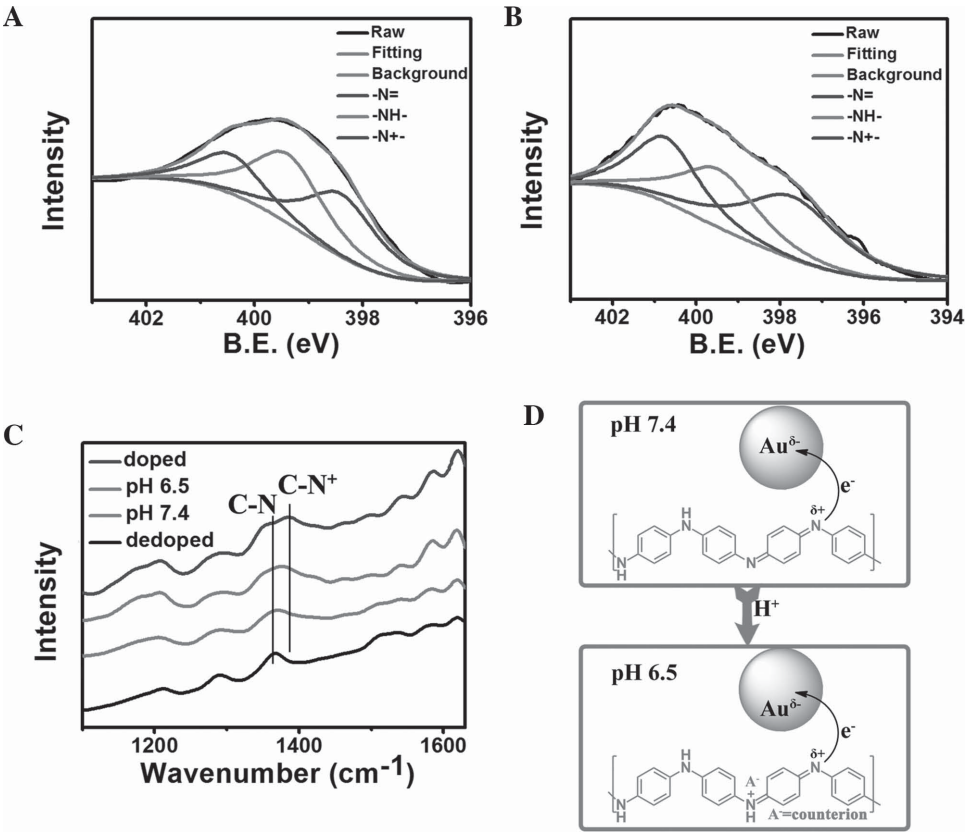

Figure 2. A) XPS N_{1s} analysis of Au@PANI in PB buffer (pH 7.4). B) XPS N_{1s} analysis of Au@PANI in PB buffer (pH 6.5). C) Raman spectra of Au@PANI in PB buffer with different pH, HCl doped PANI, and dedoped PANI. D) Proposed schematic structure of Au@PANI after pH decreased.

Au@PANI in different condition of pH by X-ray photoelectron spectra (XPS) measurement. As shown in **Figure 2**A,B, N_{1S} peak of Au@PANI could deconvolute into three discrete peaks at 398, 399.5, and 400.6 eV, which are associated with the quinoid imine, the benzenoid amine and the positively charged nitrogen, respectively. Previous studies have demonstrated that the doping process could result in a decrease in the band-gap energy and an increase in the electron-delivery efficiency, which displayed a red shift in the spectrum.[25] We then calculated the $[N^+]/[N]$ ratio through the area ratios of the peaks, which could be correlated with the doping level (N: sum of –N= , –NH–, and $–N^+–$).[42] The calculated ratio of Au@PANI at pH 6.5 was 0.36, which was higher than 0.21 of Au@PANI at pH7.4. This may due to the reason that a low pH environment favors the presence of a doped state. Besides, the strong bond between the nitrogen of the polyaniline and AuNPs led the electrons reside on the imine nitrogen of the PANI to move onto the AuNPs, which could shift the transition of PANI from pH < 3 to a higher pH.[32] To further clarify the charge transfer behavior near the nitrogen, we next employed Raman spectroscopy to observe the difference of bonding stretching. Bare PANI without AuNPs in doped and dedoped state was used as control. As shown in Figure 2C, C–C deformation bands of the benzenoid ring at 1620, 1586, and 1543 cm^{-1} were characteristic of semiquinone rings. The chemical bonds of C–N, protonated $C–N^+$ are assigned at 1354 and 1385 cm^{-1}.[43,44] Compared with dedoped PANI at peak at 1368 cm^{-1}, a broad peak and a shift to higher wave number was observed for Au@PANI at pH 7.4 (1370 cm^{-1}) and pH 6.5 (1376 cm^{-1}). This indicated that both the charge transfer from AuNPs to PANI and lower pH could improve the doping level of PANI, which was consistent with the XPS observation. Based on these results, we proposed a mechanism for the pH-dependent photothermal effect (Figure 2D). At pH 7.4, the imine nitrogen was partially positive charged due to the interaction with the AuNPs. While at pH 6.5, the introduced H^+ made imine nitrogen entirely positively charged, which greatly decreases the band-gap energy and the peak absorbance showed red-shift to NIR region. As a result, the photothermal conversion was greatly improved as the pH decreased.

We next tested the cytotoxicity and photothermal efficacy of Au@PANI at the cellular level. In vitro cytotoxicity was measured by performing methyl thiazolyl tetrazolium (MTT) assay on normal cells (HEK-293T) and the tumor cells (HepG 2 and HeLa) after incubation with Au@PANI nanoparticles at various concentrations for 24 h. Encouragingly, no significant cytotoxicity of Au@PANI was observed even the concentration reached 200 μg mL^{-1} (**Figure 3**A). The efficacy of photothermal therapy was then evaluated by incubating HepG 2 cells with Au@PANI nanoparticles at both pH 7.4 and pH 6.5 following the exposure to the 808 nm laser. As expected, the viability of cells incubated with Au@PANI at pH 6.5 with laser irradiation was decreased as the concentration

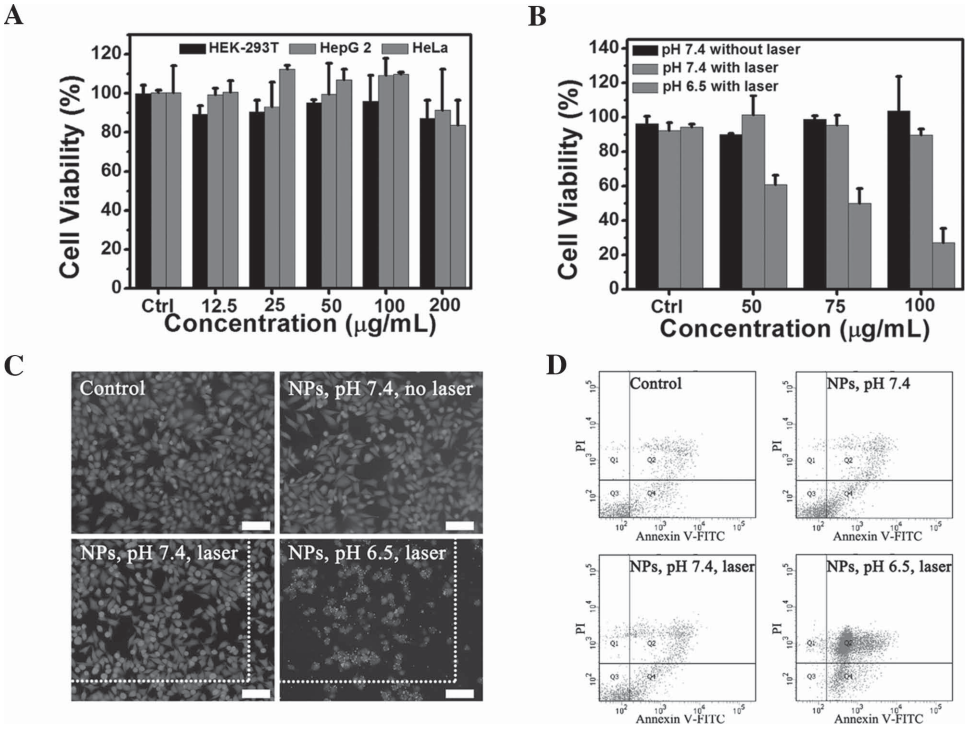

Figure 3. A) Cytotoxicity studies by MTT assay for HEK-293T, HepG 2, and HeLa cells after incubation with various concentrations of Au@PANI for 24 h. B) Relative viabilities and C) fluorescence images of calcein AM (green, live cells) and propidium iodide (red, dead cells) co-stained HepG 2 cells incubated with Au@PANI nanoparticles (NPs) at different pH with or without laser irradiation. Scale bars equal 50 μm. The rectangle sections were under irradiation. D) The corresponding flow cytometric analysis of Annexin V-FITC/PI stained cells. Cells in left lower quadrant of each picture correspond to intact cells ($FITC^-/PI^-$), cells in right lower quadrant early apoptotic cells ($FITC^+/PI^-$), cells in right upper quadrant correspond to late apoptotic/necrotic cells ($FITC^+/PI^+$).

of the Au@PANI increased (Figure 3B). The killing efficacy could reach nearly 80% when the concentration of Au@PANI reached 100 μg mL^{-1}. However, the cells incubated with Au@PANI at pH 7.4 with or without laser irradiation showed no significant change in the viability. Fluorescence imaging of cells co-stained by Calcein AM and propidium iodide confirmed the pH-dependent high efficacy of photothermal cancer cell ablation (Figure 3C). The corresponding bright field image showed shrinkage of the cell incubated with Au@PANI at pH 6.5 after laser treatment (Figure S3, Supporting Information).With the aim of visualizing cell injury through either a necrotic or apoptotic pathway, we further explored the phototoxicity by a standard annexin V-FITC/propidium iodide assay. As shown in Figure 3D, the cells incubated with Au@PANI at pH7.4 with and without laser irradiation showed a small amount of apoptosis as well as the control group, which may be attributed to the experimental operation caused cell damage. However, 83% cells incubated with Au@PANI at pH 6.5 with laser irradiation undergo late apoptosis or necrosis. This was in good agreement with the published report that temperature higher than 50 °C could evoke irreversible cell damage and necrosis.[45]

Encouraged by the in vitro performance, we proceeded to evaluate the in vivo anticancer potentials. We first measured the dynamic diameter of our nanoparticles as about 70 nm, which was suitable for prolong retention in the circulation (Figure S4, Supporting Information). The biodistribution of our nanoparticles was then investigated by intravenous injection of Au@PANI with 100 μg Au into the H22 tumor-bearing mice. The mice were sacrificed 4 h after administration and the major tissue and tumor were collected for determining the content of Au using an inductively coupled plasma mass spectrometer. We found that most of the nanoparticles accumulated in the liver and spleen, while only a small fraction retained in the tumor tissue (Figure S5, Supporting Information). Considering nanoparticles were cleared rapidly by macrophages of the reticuloendothelial system, we chose a local injection as the administration route for the most efficient delivery of photothermal agents. To demonstrate the tumor microenvironment-responsive photothermal effect of Au@PANI, we injected our nanoparticles or saline subcutaneously into the normal mice and intratumorally into tumor-bearing mice, respectively. Upon 808 nm laser irradiation (2 W cm^{-2}), thermal imaging was employed to monitor the temperature change in vivo using an infrared thermal camera (**Figure 4**A). For tumor-bearing mice injected with Au@PANI, the local tumor temperature reached over 50 °C within 5 min, which was sufficient to kill tumor cells. In comparison, the temperature of the normal mice increased to less than 45 °C under the same irradiation condition. The more rapid temperature increase in tumor may be attributed to the higher photothermal conversion efficiency of Au@PANI at more acidic tumor microenvironment. To further valid this concept, $NaHCO_3$ was used to reverse the acidic pH value of the solid

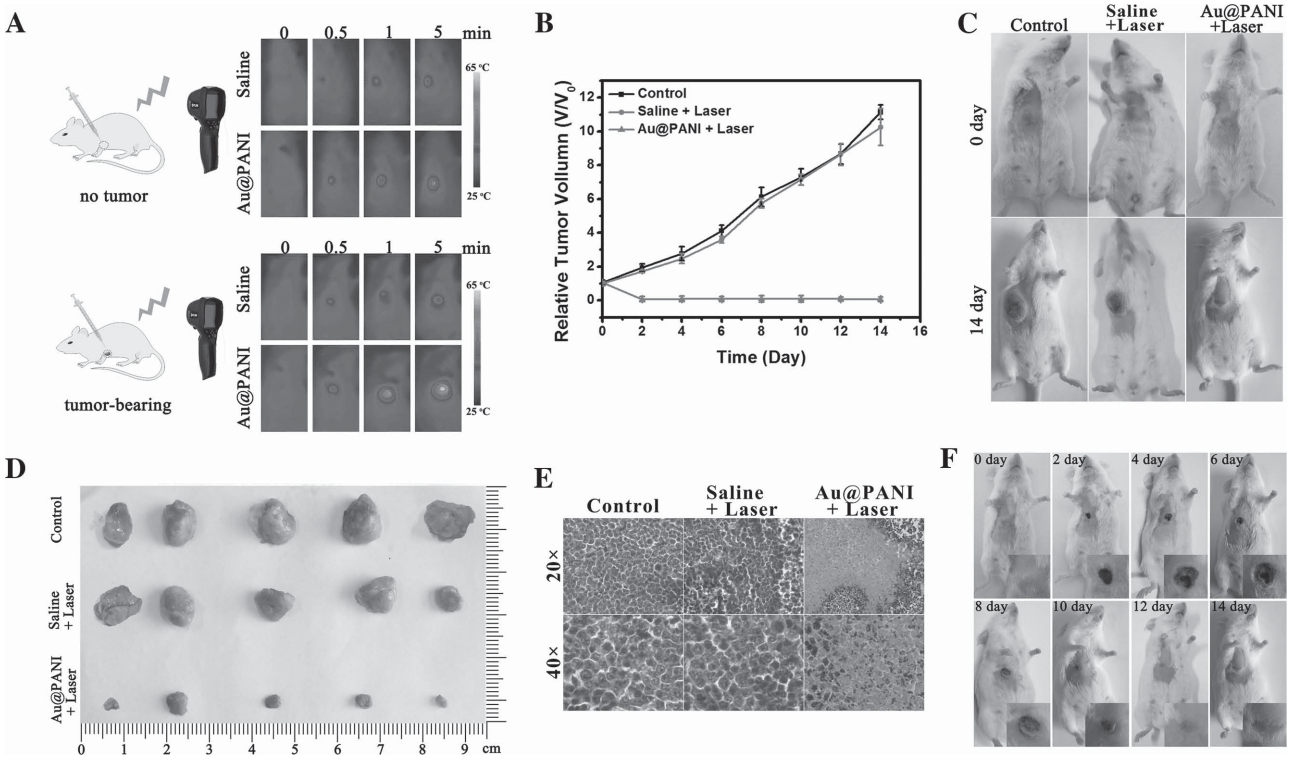

Figure 4. A) Real time in vivo IR thermal images of H22 tumor-bearing and no tumor-bearing mice with saline or Au@PANI (100 μg mL^{-1}) injection and exposure to an 808 nm laser. The power density of the laser was set as 2 W cm^{-2}. B) Relative tumor volume after various treatments indicated. Error bars represent the standard deviations of 5 mice per group. C) Photographs of the H22 tumor-bearing mice before treatment and on day 14 after the various treatments. D) Representative photographs of the tumor dissection. E) Hematoxylin and eosin (H&E) staining of tumor sections collected from the mice after 1 day treatment. F) Typical photographs of H22 tumor-bearing mice at different days after Au@PANI injection and 808 nm laser irradiation. Inserted were the amplified sections of the tumors.

tumor. After the tumor-bearing mice co-injected with Au@PANI and $NaHCO_3$ and irradiated with NIR laser, the temperature change was similar to that of mice injected with saline (Figure S6, Supporting Information). As a result, the tumor microenvironment activated photothermal effect could minimize damage to normal tissues without regard to the precisely operation of laser irradiation on cancer cells. Remarkably, the tumors injected with Au@PANI after irradiation treatment showed complete tumor regression compared to the control or laser only groups after 2 weeks (Figure 4B–D). Especially, the ablated tumors became black scars at the original sites and showed no reoccurrence after the scars fell off the skin (Figure 4F). The mice could survive over 40 days once the treatment started (Figure S7, Supporting Information). Tumor tissues were collected after 1 day after irradiation for histopathological examination by staining with hematoxylin and eosin (H&E) (Figure 4E). In the Au@PANI with irradiation group, condensation of chromatin and nuclear fragmentations could be found, indicating the intensive necrosis or apoptosis of the cancer cells. Moreover, no significant body weight variation was observed after the photothermal treatment (Figure S8, Supporting Information). In addition, no obvious damage or inflammation was observed in the major organs after the photothermal treatment (Figure S9, Supporting Information). These results indicating that Au@PANI have great potential to act as a tumor microenvironment activated photothermal agent for effective cancer therapy.

3. Conclusion

In conclusion, we have demonstrated a tumor microenvironment activated photothermal strategy based on pH-dependent light-heat conversion property of Au@PANI nanoparticles. Compared with traditional photothermal therapy, the tumor microenvironment-activated photothermal therapy exhibited highly discriminating photoinduced damage to tumor region while leaving normal tissues intact. Importantly, with the benefit of the internal and external control to switch on the photothermal ablation, technical difficulty to precisely operate laser irradiation on tumor cells could be circumvented. Considering the microenvironment in tumors have other differences from that in normal tissue, such as hypoxia and matrix metalloproteinase enzymatic activity, we anticipate that the activated photothermal strategy will provide opportunities to explore more intelligent platform for solid tumor ablation.

Supporting Information

Supporting Information is available from the Wiley Online Library or from the author.

Acknowledgements

Financial support was provided by National Basic Research Program of China (Grant Nos. 2012CB720602 and 2011CB936004) and the National Natural Science Foundation of China (Grant Nos. 21210002, 21303182, 21431007, and 91413111).

Received: November 4, 2014
Revised: December 22, 2014
Published online: January 28, 2015

[1] X. H. Huang, P. K. Jain, I. H. El-Sayed, M. A. El-Sayed, *Laser Med. Sci.* **2008**, *23*, 217.
[2] S. Lal, S. E. Clare, N. J. Halas, *Acc. Chem. Res.* **2008**, *41*, 1842.
[3] L. Cheng, C. Wang, L. Z. Feng, K. Yang, Z. Liu, *Chem. Rev.* **2014**, *114*, 10869.
[4] R. Weissleder, *Nat. Biotechnol.* **2001**, *19*, 316.
[5] X. H. Gao, Y. Y. Cui, R. M. Levenson, L. W. K. Chung, S. M. Nie, *Nat. Biotechnol.* **2004**, *22*, 969.
[6] V. J. Pansare, S. Hejazi, W. J. Faenza, R. K. Prud'homme, *Chem. Mater.* **2012**, *24*, 812.
[7] L. Dykman, N. Khlebtsov, *Chem. Soc. Rev.* **2012**, *41*, 2256.
[8] L. Cheng, K. Yang, Y. G. Li, J. H. Chen, C. Wang, M. W. Shao, S. T. Lee, Z. Liu, *Angew. Chem. Int. Ed.* **2011**, *50*, 7385.
[9] W. J. Dong, Y. S. Li, D. C. Niu, Z. Ma, J. L. Gu, Y. Chen, W. R. Zhao, X. H. Liu, C. S. Liu, J. L. Shi, *Adv. Mater.* **2011**, *23*, 5392.
[10] K. Yang, L. Z. Feng, X. Z. Shi, Z. Liu, *Chem. Soc. Rev.* **2013**, *42*, 530.
[11] Q. W. Tian, M. H. Tang, Y. G. Sun, R. J. Zou, Z. G. Chen, M. F. Zhu, S. P. Yang, J. L. Wang, J. H. Wang, J. Q. Hu, *Adv. Mater.* **2011**, *23*, 3542.
[12] K. Dong, Z. Liu, Z. H. Li, J. S. Ren, X. G. Qu, *Adv. Mater.* **2013**, *25*, 4452.
[13] X. J. Yang, X. Liu, Z. Liu, F. Pu, J. S. Ren, X. G. Qu, *Adv. Mater.* **2012**, *24*, 2890.
[14] J. Tian, L. Ding, H. Ju, Y. Yang, X. Li, Z. Shen, Z. Zhu, J. S. Yu, C. J. Yang, *Angew. Chem. Int. Ed.* **2014**, *53*, 9544.
[15] P. Huang, P. Rong, A. Jin, X. Yan, M. G. Zhang, J. Lin, H. Hu, Z. Wang, X. Yue, W. Li, G. Niu, W. Zeng, W. Wang, K. Zhou, X. Chen, *Adv. Mater.* **2014**, *26*, 6401.
[16] S. P. Sherlock, H. J. Dai, *Nano Res.* **2011**, *4*, 1248.
[17] N. E. Sounni, A. Noel, *Clin. Chem.* **2013**, *59*, 85.
[18] O. Tredan, C. M. Galmarini, K. Patel, I. F. Tannock, *J. Natl. Cancer Inst.* **2007**, *99*, 1441.
[19] C. Ward, S. P. Langdon, P. Mullen, A. L. Harris, D. J. Harrison, C. T. Supuran, I. H. Kunkler, *Cancer Treat Rev.* **2013**, *39*, 171.
[20] W. R. Wilson, M. P. Hay, *Nat. Rev. Cancer* **2011**, *11*, 393.
[21] X. S. Liu, Y. J. Chen, H. Li, N. Huang, Q. Jin, K. F. Ren, J. Ji, *ACS Nano* **2013**, *7*, 6244.
[22] J. N. Liu, Y. Liu, W. B. Bu, J. W. Bu, Y. Sun, J. L. Du, J. L. Shi, *J. Am. Chem. Soc.* **2014**, *136*, 9701.
[23] P. Prasad, C. R. Gordijo, A. Z. Abbasi, A. Maeda, A. Ip, A. M. Rauth, R. S. DaCosta, X. Y. Wu, *ACS Nano* **2014**, *8*, 3202.
[24] Q. N. Lin, C. Y. Bao, Y. L. Yang, Q. N. Liang, D. S. Zhang, S. Y. Cheng, L. Y. Zhu, *Adv. Mater.* **2013**, *25*, 1981.
[25] J. Yang, J. Choi, D. Bang, E. Kim, E.-K. Lim, H. Park, J.-S. Suh, K. Lee, K.-H. Yoo, E.-K. Kim, Y.-M. Huh, S. Haam, *Angew. Chem. Int. Ed.* **2011**, *50*, 441.
[26] T. Lee, D. Bang, Y. Park, S. H. Kim, J. Choi, J. Park, D. Kim, E. Kim, J.-S. Suh, Y.-M. Huh, S. Haam, *Adv. Healthcare Mater.* **2014**, *3*, 1408.
[27] A. Malinauskas, *J. Power Sources* **2004**, *126*, 214.
[28] J. Yue, Z. H. Wang, K. R. Cromack, A. J. Epstein, A. G. Macdiarmid, *J. Am. Chem. Soc.* **1991**, *113*, 2665.
[29] S. A. Chen, G. W. Hwang, *J. Am. Chem. Soc.* **1995**, *117*, 10055.
[30] H. Zengin, W. S. Zhou, J. Y. Jin, R. Czerw, D. W. Smith, L. Echegoyen, D. L. Carroll, S. H. Foulger, J. Ballato, *Adv. Mater.* **2002**, *14*, 1480.
[31] E. Coşkun, E. A. Zaragoza-Contreras, H. J. Salavagione, *Carbon* **2012**, *50*, 2235.
[32] R. J. Tseng, J. X. Huang, J. Ouyang, R. B. Kaner, Y. Yang, *Nano Lett.* **2005**, *5*, 1077.
[33] E. Granot, E. Katz, B. Basnar, I. Willner, *Chem. Mater.* **2005**, *17*, 4600.
[34] J. Kundu, O. Neumann, B. G. Janesko, D. Zhang, S. Lal, A. Barhoumi, G. E. Scuseria, N. J. Halas, *J. Phys. Chem. C* **2009**, *113*, 14390.
[35] H. Chi, B. H. Liu, G. J. Guan, Z. P. Zhang, M. Y. Han, *Analyst* **2010**, *135*, 1070.
[36] X. F. Zhang, H. Zhao, Y. Xue, Z. J. Wu, Y. Zhang, Y. J. He, X. J. Li, Z. B. Yuan, *Biosens. Bioelectron.* **2012**, *34*, 112.
[37] J. van der Zee, *Ann. Oncol.* **2002**, *13*, 1173.
[38] S. Yokota, M. Kitahara, K. Nagata, *Cancer Res.* **2000**, *60*, 2942.
[39] D. Yoo, H. Jeong, S. H. Noh, J. H. Lee, J. Cheon, *Angew. Chem. Int. Ed.* **2013**, *52*, 13047.
[40] L. E. Ibarra, E. I. Yslas, M. A. Molina, C. R. Rivarola, S. Romanini, C. A. Barbero, V. A. Rivarola, M. L. Bertuzzi, *Laser Phys.* **2013**, *23*, 066004.
[41] J. Zhou, Z. Lu, X. Zhu, X. Wang, Y. Liao, Z. Ma, F. Li, *Biomaterials* **2013**, *34*, 9584.
[42] B. J. Kim, S. G. Oh, M. G. Han, S. S. Im, *Langmuir* **2000**, *16*, 5841.
[43] K. Mallick, M. J. Witcomb, A. Dinsmore, M. S. Scurrell, *Macromol. Rapid Commun.* **2005**, *26*, 232.
[44] R. J. Tseng, C. O. Baker, B. Shedd, J. X. Huang, R. B. Kaner, J. Y. Ouyang, Y. Yang, *Appl. Phys. Lett.* **2007**, *90*, 053101.
[45] B. V. Harmon, A. M. Corder, R. J. Collins, G. C. Gobe, J. Allen, D. J. Allan, J. F. R. Kerr, *Int. J. Radiat. Biol.* **1990**, *58*, 845.